560

Journal of Hydrology, 102 (1988) 335-354
Elsevier Science Publishers B.V., Amsterdam — Printed in The Netherlands

[1]

EFFECT OF STORM RAINFALL INTENSITY PATTERNS ON SURFACE RUNOFF

D.A. WOOLHISER and D.C. GOODRICH

U.S. Department of Agriculture, Aridland Watershed Management Research Unit, 2000 East Allen Road, Tucson, AZ 85719 (U.S.A.)
Agricultural Research Service, U.S. Department of Agriculture, and *Department of Hydrology and Water Resources, University of Arizona, Tucson, Ariz. (U.S.A.)*

(Received April 1, 1987; accepted after revision June 26, 1987; received at publisher March 11, 1988)

ABSTRACT

Woolhiser, D.A. and Goodrich, D.C., 1988. Effect of storm rainfall intensity patterns on surface runoff. In: R.L. Bras, M. Hino, K. Takeuchi and P.K. Kitanidis (Editors), Hydrologic Research: The U.S.-Japan Experience. J. Hydrol., 102: 335-354.

The adoption of physically-based infiltration models as components of watershed models has been impeded because they require rainfall data with high temporal and spatial resolution, and the spatial variability of infiltration model parameters must be accounted for. Techniques have been developed to disaggregate daily rainfall into the intermittent shower process within the day, and further disaggregate significant showers into short-period rainfall hyetographs. A simple model describing infiltration and unsteady flow over a plane and a single channel is used to investigate the sensitivity of derived distributions of runoff volume and peak flow rates to input differences due to different rainfall disaggregation methods and parameters and to spatial variability of infiltration parameters. The Woolhiser and Osborn disaggregation scheme is superior to simpler forms of disaggregation for all but a highly damped system. For the elementary watershed considered, the channel has little effect on basis response in comparison to overland flow characteristics. A significant interaction between climate and spatially variable infiltration and its effects on response was also discovered and is discussed.

INTRODUCTION

The adoption of physically-based infiltration models as components of watershed models has been hampered by the problem of spatial variability of infiltration parameters and the requirement for rainfall data with high spatial and temporal resolution. Although both problems have been studied for a number of years, there are no definitive guidelines available for determining the appropriate spatial and temporal resolution required for rainfall inputs to distributed runoff models or the spatial resolution required for infiltration parameters.

Eagleson and Shack (1966) developed sampling-interval criteria for thunderstorm and cyclonic rainfall, which depend on the relationship between the

0022-1694/88/$03.50 © 1988 Elsevier Science Publishers B.V.

passband frequency of the drainage basin model and the band width of the precipitation signal. Harley et al. (1970) recommended a rainfall sampling interval of $t_c/3.2$ where t_c is the kinematic time to equilibrium for the basin at some characteristic runoff rate. Bras (1979) reviewed the literature on sampling interrelated hydrologic random fields, and pointed out that the most significant limitations of previous work are associated with the definition of storm duration and depth and the neglect of the effects of infiltration. Woolhiser (1986) verified that the criterion of Harley et al. (1970) is appropriate for impervious basins, but is not adequate if infiltration is calculated with an interactive infiltration model.

These studies on the appropriate rainfall sampling intervals are helpful where analog raingage data are available, or where raingages are to be installed, but frequently, only daily rainfall data are available. In this situation, physically-based infiltration models cannot be used at present. Research on daily rainfall disaggregation has recently been initiated. The objective of this work is to develop the stochastic model structure and parameter values from the relatively few locations where "breakpoint" rainfall data are available, and to use this model in the simulation mode to disaggregate existing daily rainfall data into short-period rainfall intensities.

Two approaches have been used. The first, which we will call discrete–discrete (D–D), consists of a model to disaggregate the discrete process of daily rainfall into the discrete process of hourly rainfall, and a second model to disaggregate hourly rainfall into 6-min rainfall. The second approach, which we shall call discrete–continuous (D–C), consists of a model to disaggregate daily rainfall into the continuous process of showers and dry periods within the day, and a second model to disaggregate the showers into short-term rainfall intensities. The D–D method is exemplified by the work of Srikanthan and McMahon (1985), while Woolhiser et al. (1985), Woolhiser and Osborn (1985), and Hershenhorn (1984) use the D–C method. The D–C method seems to have a potential advantage in that it apparently requires fewer parameters. However, the problems of how to account for seasonality in parameters and the degree of time resolution required still remain. These are crucial problems which will have a major impact on the number of parameters required, and, in turn, may decide the feasibility of the disaggregation approach.

The objective of this paper is to extend previous studies by examining the effect of damping by channel routing and spatial variation of infiltration on the interaction between rainfall intensity patterns, infiltration, basin response time, and the distribution of peak runoff rates, runoff volumes, and time to peak. This study will be limited to Hortonian overland flow over simple geometric arrangements of planes and channels.

THE RAINFALL–RUNOFF MODEL

Overland flow is described by the kinematic wave equation for flow over a plane of length L:

$$\frac{\partial h}{\partial t} + \frac{\partial \alpha h^m}{\delta x} = r_i(t) - f_i(t) \tag{1}$$

where: h is the average depth per unit area averaged over some characteristic area; t is time; x is the distance along the slope; $r_i(t)$ is the rainfall rate; and $f_i(t)$ is the infiltration rate. If flow resistance is approximated by the Manning law, the parameter $\alpha = S^{1/2}/n$, where S is the slope of the plane, $m = 5/3$ and n is the Manning coefficient.

Unsteady channel flow is also described by the kinematic wave equation:

$$\frac{\partial A}{\partial t} + \frac{\partial Q(A)}{\partial x} = q_1 \tag{2}$$

where: A is the wetted cross-sectional area; $Q(A)$ is the channel discharge rate as a function of area A; and q_1 is the uniform lateral inflow from contributing planes. The Manning equation is also used for channel flow and the channel is chosen to be sufficiently wide, such that the hydraulic radius $R \approx h$. Dry initial conditions are assumed for both planes and channels, and the upper boundary conditions are $h(0,t) = 0$ and $A(0,t) = 0$.

Infiltration is described by the Smith–Parlange (1978) model, which is based on an approximation to the Richards equation describing one-dimensional unsaturated flow in a homogeneous porous medium. The Smith–Parlange model states that at the ponding time, t_p:

$$\int_0^{t_p} r_i(t)\mathrm{d}t = (A/K_s')\ln\{r_i(t_p)/[r_i(t_p) - K_s']\} = F_p \tag{3}$$

where: K_s' is the effective saturated hydraulic conductivity under inhibition; A is a parameter related to the sorptivity; and F_p is depth (volume per unit area) of precipitation that has fallen prior to ponding and infiltrated.

After ponding, $r_i(t)$ in eqn. (3) can be replaced with $f_i(t)$, and the following implicit relationship between the accumulated infiltration, F, and time can be derived (Smith and Parlange, 1978):

$$K_s'(t - t_p) = F - F_p + A_p\exp(-F/A_p) - A_p[r_i(t_p) - K_s']/r_i(t_p) \tag{4}$$

where $A_p = A/K_s'$. The parameter A can be estimated from the soil sorptivity S:

$$A = S^2/2 \tag{5}$$

Freeze (1980) concluded that the distribution of hydraulic conductivities should be incorporated into physically based rainfall–runoff models. This has been accomplished in a simple and straight forward manner in this study. The effective saturated hydraulic conductivity, K_s', is assumed to be a log-normally distributed random variable. Let $z = \ln K_s'$. The random variable z is assumed to be normally distributed with mean $\bar{z}$ and variance S_z^2. The statistical characteristics of K_s' are specified by the geometric mean, $\exp(\bar{z})$, and the coefficient

of variation of z, $S_z/\bar{z}$. The variability of K_s' is accounted for by assuming that each plane is subdivided into five parallel planes with widths equal to one fifth of the original plane width. The K_s' value assigned to each plane corresponds to the midpoint of each of five equal probability classes. Although the spatial correlation structure of K_s' is not preserved, it appears that this is not a major shortcoming (Freeze, 1980).

Review of the literature (Russo and Bresler, 1981; Grah et al., 1983; Loague, 1986) reveals that the typical range of significant spatial correlation of hydraulic conductivities is on the order of 10–20 m on uncultivated soil. Therefore, if the width of an overland flow plane used in modeling is greater than 80–100 m, the assumption of independence of the five plane segments should not be a serious oversimplification.

ANALYSES

A Monte Carlo simulation approach was used to study the effect of storm rainfall intensity patterns on certain characteristics of surface runoff hydrographs. The geometry of the simple catchment used in this study is shown schematically in Fig. 1, and corresponds to that used by Iwagaki and Takasao (1956), Ishihara and Takasao (1963), and Wooding (1965a). The methodology employed in this study can be described by the diagram in Fig. 2. The true rainfall intensity process at a point in space, $R_i(t)$, is measured in a weighing-recording raingage, and the accumulated depths at unequal time increments are determined from the analog charts and digitized, resulting in the "breakpoint" data $r_i(t)$. We used data from raingage no. 5 at the Walnut Gulch Experimental Watershed in southeastern Arizona, U.S.A. This gage is a dual-traverse, weighing recording gage with a depth resolution of approximately 0.15 mm ± 0.30 mm, and has a time resolution of 2.5 min ± 5 min. The 30 largest storms that occurred in a 23-year period of record were used in the study. These storms are characteristic of air mass thunderstorm rainfall and are a subset of the "geographically centered" data used by Woolhiser and

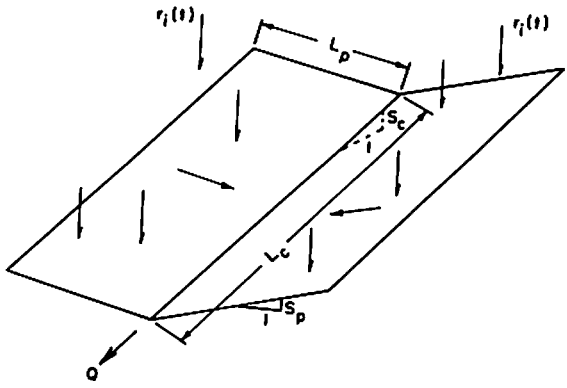

Fig. 1. Catchment geometry.

Osborn (1985). The storms have been truncated by cutting off portions of the storm at the beginning or end when intensities were below $3\,\mathrm{mm\,h^{-1}}$ ($0.12\,\mathrm{in\,h^{-1}}$). These "tails" seldom amount to more than 5% of the total storm rainfall, but can add substantially to the storm duration. Each of the storms, as represented by the breakpoint data, $r_i(t)$, were used as rainfall input to the runoff model, and for each event, k, the volume of runoff, V_k, the peak rate of runoff, Q_k, and the time to peak, T_{Qk}, were calculated. These sample points were then ordered and plotting positions calculated. The sample distribution functions obtained in this manner were used as a standard for an empirical investigation of the effect of the temporal patterns of storm rainfall on the distribution of runoff volume, rates, and time to peak.

As indicated in Fig. 2, three additional storm sequences were used as rainfall input to the runoff model. For each of these sequences, the rainfall depth and duration were preserved for each storm. The sequences consisted of the following:

(1) Rainfall intensities obtained using the disaggregation method described by Woolhiser and Osborn (1985). The parameters for the disaggregation model were estimated using 242 storms which occurred during July and August at the Walnut Gulch Experimental Watershed in southeastern Arizona.

(2) Rainfall intensities obtained by a step function approximation to an isosceles triangle. Engman and Hershfield (1981) have used a triangular representation for the intensity pattern of storms shorter than 2 h.

(3) Constant intensity within each storm, with the intensity equal to the storm depth divided by the duration. This approach has been used previously in deriving analytic expressions for flood frequency distributions (Eagleson,

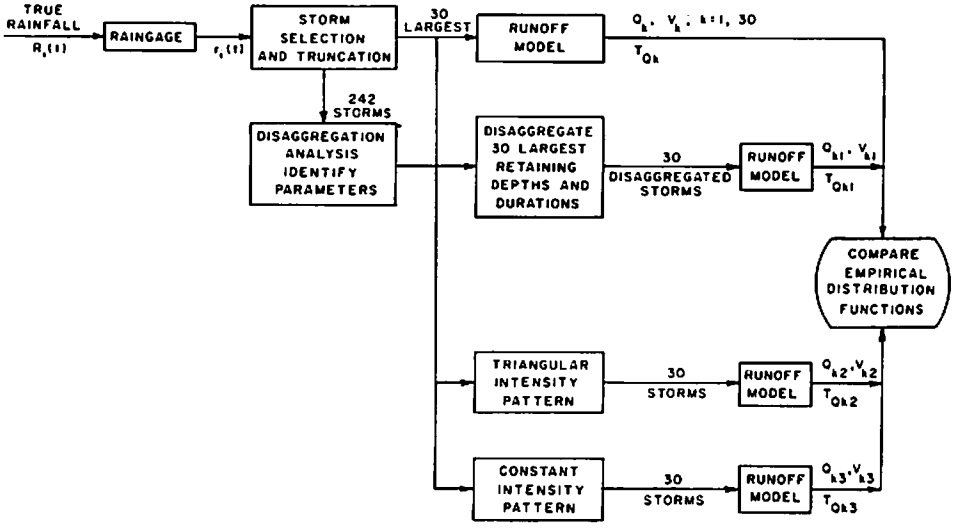

Fig. 2. Schematic diagram of methodology.

1972). Sample distribution functions of runoff volume, peak rate, and time to peak were obtained for each of these input series for each combination of basin geometry and infiltration parameter set, and were compared with those obtained with real breakpoint data as input.

To reduce the number of simulations required, the relationships between the watershed response time, infiltration characteristics, and the precipitation input are described by four dimensionless ratios. The first dimensionless number, T_*, is the ratio of the time to kinematic equilibrium on the overland flow plane to the mean duration of the set of 30 storms ($\bar{D}$):

$$T_* = t_e/\bar{D} = (nL\,S^{-0.5}\,\bar{q}^{-0.67})^{0.6}/\bar{D} \tag{6}$$

where $\bar{q}$, the mean storm intensity, is equal to:

$$1/m \sum_{k=1}^{m} P_k/D_k$$

P_k and D_k are the total rainfall and the duration of the kth storm, respectively, n is Manning's roughness coefficient, and S is the slope of the plane. The second dimensionless number, λ, is that used by Wooding (1965a) to characterize the relative importance of channel flow and overland flow. It is a ratio of the kinematic time to equilibrium in the channel to the time to equilibrium on the contributing overland flow plane:

$$\lambda = \frac{1}{t_{ep}}\left[\frac{L_c}{\alpha_c}\right]^{1/m}\left[2\bar{q}L_p\right]^{(1-m)/m} \tag{7}$$

where L_c is the channel length, t_{ep} is the time to equilibrium on the plane, and α_c is obtained by assuming a Manning flow law for uniform flow in a rectangular channel.

α_c is first defined by the relationship:

$$Q_c = \alpha_c A_c^m \tag{8}$$

$$Q_c = 1/n_c(S_c)^{1/2}\,H_c^{5/3}\,W_c \tag{9}$$

where: Q_c = discharge in the channel; n_c = Manning's roughness coefficient for the channel; S_c = channel slope; H_c = flow depth; and W_c is the channel width. It is also assumed that $W_c \gg H_c$, so that $H_c \approx$ hydraulic radius. To satisfy the power relation in eqns. (8) and (9), α_c and m must be:

$$\alpha_c = 1/n_c\,S_c^{1/2}\,W_c^{\,2/3} \tag{10}$$

$$m = 5/3 \tag{11}$$

It should be noted that T_* and λ relate only to the hydraulic response characteristics of the catchment. However, they do incorporate the characteristics of the storm set, so will vary regionally in response to the rainfall regime.

The second two dimensionless ratios describe the interaction between the infiltration characteristics and the storm set. The infiltration depth ratio F_{p*} is

defined as the ratio of the infiltrated depth at ponding, F_p, to the mean storm depth:

$$F_{p^*} = F_p/\bar{P} = F_p \Big/ \left[1/m \sum_{k=1}^{m} P_k \right] \tag{12}$$

where F_p is obtained from eqn. (3) with the soil at a dry initial condition and the rainfall rate assumed to be constant at the mean storm intensity $\bar{q}$. The second ratio related to infiltration is C_v, the coefficient of variation of ln K_s'. CV is dependent only on the catchment soil characteristics, while F_{p^*} is dependent on both soil characteristics and the storm set.

The statistical characteristics of the storm set used in this study are given in Table 1. Catchment and infiltration characteristics were chosen to cover a substantial range of response time and soil textures. The time to equilibrium on the plane, t_{ep}, ranged from 1.63 min (insuring that the maximum peak runoff rate from a plane with an impervious surface is the same as the maximum intensity for the storm) to 27.7 min. The channel response time ranged from 0 (plane only) to $1.5t_{ep}$, with increments of $0.5t_{ep}$. Infiltration ranged from zero (impervious plane) to that consistent with a sandy loam soil. CV ranged from zero (homogeneous soil) to 0.8. Infiltration parameter values were calculated from the table presented by Rawls et al. (1982) using the approximations:

$$A_p = 0.5\,(2 + 3\beta)P_b(S_{max} - S_i)\phi/(1 + 3\beta) \tag{13}$$

and:

$$K_s' = K_s/2 \tag{14}$$

where: β is the pore size distribution index, ϕ is porosity, P_b is the bubbling pressure, S_{max} and S_i are the maximum soil water content under imbibition and the initial soil water content, respectively, and K_s is the saturated hydraulic conductivity. See Smith and Parlange (1978) and Brakensiek (1977) for explanations of these approximations. S_i was always assumed to be zero.

Dimensional and dimensionless parameter values for the cases investigated are shown in Table 2.

RESULTS

Spatially uniform infiltration rate

The effects of rainfall intensity patterns, catchment response characteristics, and infiltration on the distribution functions of peak runoff rates, runoff volumes, and time to peak were first investigated with infiltration parameters assumed to be spatially uniform. Results are presented first for impervious catchments with rapid response times, then the effect of increasing the response time is demonstrated, and, finally, the effects of increasing infiltration rates are shown.

Empirical cumulative distribution functions (CDFs) of peak discharge rate,

TABLE 1

Statistical characteristics of storm set

	Depth (mm)	Duration (min)	Intensity (mm h^{-1})
Mean	25.9	47.4	35.7
Standard deviation	13.3	20.7	
Median	22.1	44.0	

TABLE 2

Selected plane and channel model parameters

Case	Length of plane (m)	Spatially uniform infiltration rate					
		S_p	n_p	t_{cp} (min)	T_*	F_{p*}	λ
1–4	30.48	0.10	0.01	1.63	0.0345	0.0	0.0, 0.5, 1.0, 1.5
5–8	152.4	0.005	0.05	27.67	0.585	0.0	0.0, 0.5, 1.0, 1.5
9–12	30.48	0.10	0.01	1.63	0.0345	0.104	0.0, 0.5, 1.0, 1.5
13–16	30.48	0.10	0.01	1.63	0.0345	1.15	0.0, 0.5, 1.0, 1.5
17–20	30.48	0.10	0.01	1.63	0.0345	0.290	0.0, 0.5, 1.0, 1.5
21–24	152.4	0.005	0.05	27.67	0.585	0.104	0.0, 0.5, 1.0, 1.5
25–28	152.4	0.005	0.05	27.67	0.585	0.290	0.0, 0.5, 1.0, 1.5
29–32	152.4	0.005	0.05	27.67	0.585	1.15	0.0, 0.5, 1.0, 1.5
33–36	152.4	0.005	0.05	27.67	0.585	0.590	0.0, 0.5, 1.0, 1.5
37–40	91.4	0.03	0.07	14.56	0.308	0.0	0.0, 0.5, 1.0, 1.5
41–44	91.4	0.03	0.07	14.56	0.308	1.26	0.0, 0.5, 1.0, 1.5
45–48	91.4	0.03	0.07	14.56	0.308	0.574	0.0, 0.5, 1.0, 1.5

Case	Length of plane (m)	Spatially variable infiltration rate						
		S_p	n_p	t_{cp} (min)	T_*	F_{p*}	λ	$CV(\ln K'_s)$
49–51	152.4	0.005	0.05	27.67	0.585	0.104	0.0	0.0, 0.4, 0.8
52–54	152.4	0.005	0.05	27.67	0.585	0.574	0.0	0.0, 0.4, 0.8
55–57	152.4	0.005	0.05	27.67	0.585	1.26	0.0	0.0, 0.4, 0.8
58–60	91.4	0.03	0.07	14.56	0.308	0.104	0.0	0.0, 0.4, 0.8
61–63	91.4	0.03	0.07	14.56	0.308	0.574	0.0	0.0, 0.4, 0.8
64–66	91.4	0.03	0.07	14.56	0.308	1.264	0.0	0.0, 0.4, 0.8

Q, for a rapidly-responding, impervious catchment, are shown in Fig. 3. It is clear that λ has very little effect on the CDF with breakpoint (BP) rainfall input, and that the constant (CP) and triangular (TP) intensity patterns result in highly biased CDFs. THE CDF obtained using the Woolhiser and Osborn (1985) (WO) method agrees reasonably well at the lower rates, but is biased low

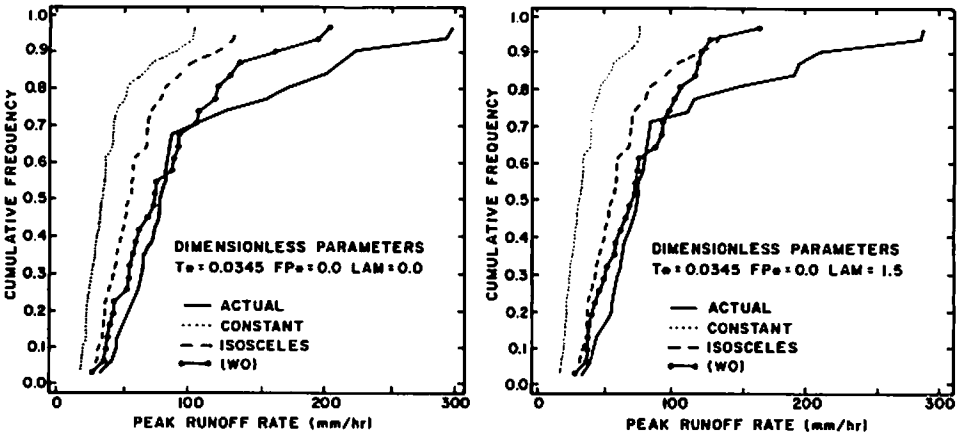

Fig. 3. Empirical CDFs of peak discharge for a 30.5 m impervious plane for varying λ (Cases 1 and 4, Table 2).

on the upper tail. The small effect of λ can be explained by the fact that the time resolution of the actual storms (from breakpoint data) is greater than the equilibrium time of the plane (1.67 min), so the peak rates of runoff from the planes are equal to the peak rainfall rates. Even with λ of 1.5, the total time to equilibrium is only about 4 min, so peak runoff rates would be less than peak rainfall rates only if the duration of the peak rainfall rate were less than 4 min.

The CDFs for a slowly-responding impervious catchment, shown in Fig. 4, demonstrate a point that has been made by Hjelmfelt (1981); namely, that if the response time of the system is longer than the total duration of the rainfall excess, the peak runoff rate depends only on the depth of rainfall, and the

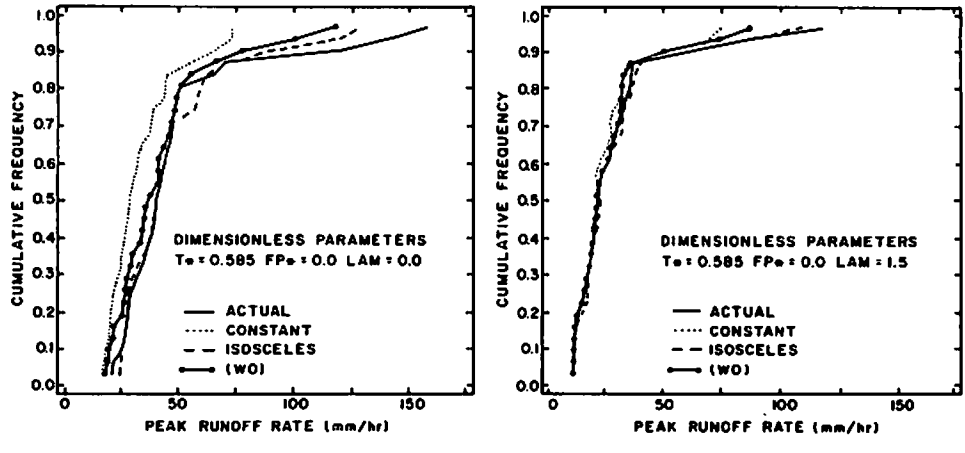

Fig. 4. Empirical CDFs of peak discharge for a 152.4 m impervious plane for varying λ (Cases 5 and 8, Table 2).

intensity distribution has no effect at all. Because t_{ep} for this case is 27.6 min, a λ of 1.5 results in a total equilibrium time of about 69 min, which is longer than many of the storms. The apparent superiority of the WO disaggregation over CP and TP inputs has also disappeared, as would be expected. It should be noted that the WO method provides a sequence of storm patterns which are dependent on the number chosen to seed the random number generator at the beginning of the simulation sequence (the sampling variability introduced by this factor is addressed later).

The effects of infiltration on the CDFs are shown in Figs. 5 and 6. The CDFs for a catchment with 91.4 m planes and a dry silt loam soil are shown in Fig. 5. The time to equilibrium, t_{ep}, is 14.6 min, significantly greater than the time

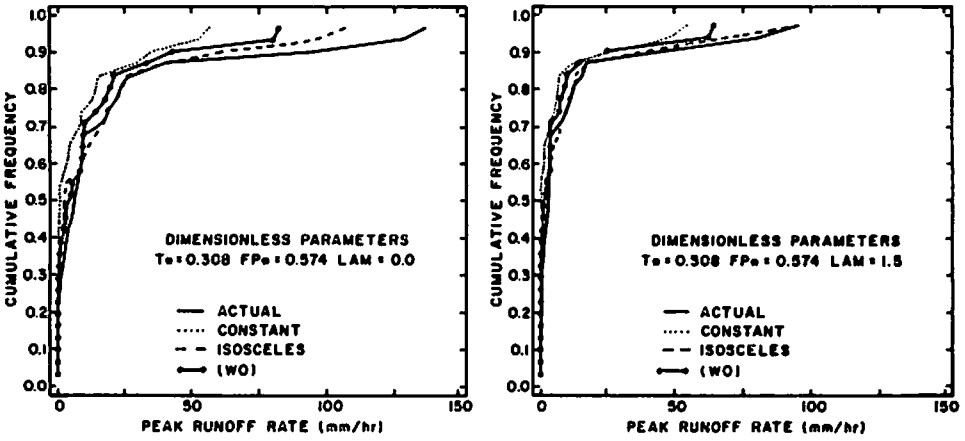

Fig. 5. Empirical CDFs of peak discharge for a 91.4 m plane with dry silt loam soil for varying λ (Cases 45 and 48, Table 2).

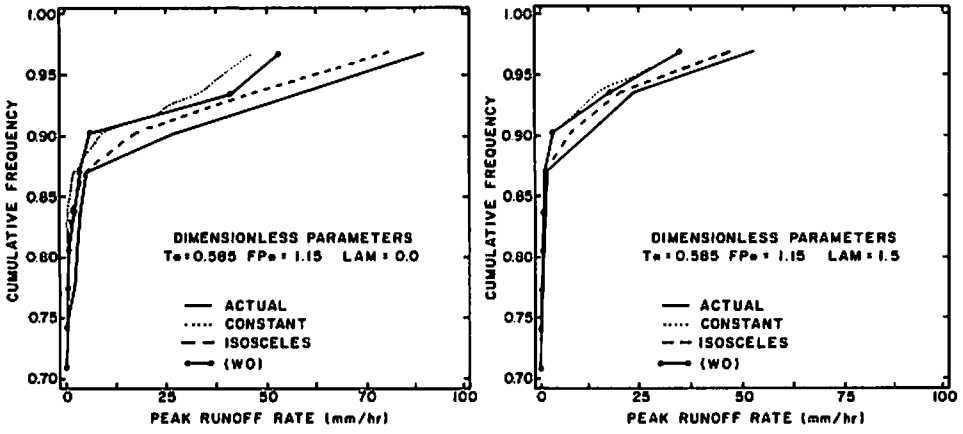

Fig. 6. Empirical CDFs of peak discharge for a 152.4 m plane with high infiltration for varying λ (Cases 29 and 32, Table 2).

resolution of the storm set. This increase in t_{cp}, and the infiltration losses, cause the CDFs to be closer together than they are in Fig. 3, and the CDFs converge further as λ increases. Figure 6 presents CDFs for the upper extreme values of T_* and F_{p*} for two levels of λ. Note that, with large F_{p*} (1.15), many of the storms do not produce runoff, so only the cumulative frequency range from 0.7 to 1.0 is shown. For purposes of this study, an event was considered to produce zero runoff if the calculated runoff volume, in inches over the basin, was less than the measuring resolution of the raingages (0.15 mm or 0.006 in).

In an attempt to quantify the effect of changes in the three dimensionless parameters on the derived CDFs for Q, the Kolmogorov–Smirnov (K–S) D_* statistic was computed for each of the cases:

$$D_* = \max [|F(Q) - F_i(Q)|], \quad i = 1, 2, 3 \tag{15}$$

where $F(Q)$ = the CDF of peak runoff rate using breakpoint input data, and $F_i(q)$ = the CDF of peak runoff rate using rainfall input from one of the three alternative rainfall patterns.

Because the samples are not independent (the same sequence of durations and amounts of rainfall were used to obtain each peak runoff series), D_* cannot be used for hypotheses testing. However, it does provide a convenient measure of differences between sample distribution functions. Contour plots of D_* versus T_* and F_{p*} for each level of λ for the constant intensity input are shown in Fig. 7. Similar plots are presented for TP and WO input patterns in Figs. 8 and 9, respectively. An inspection of these figures reveals that the WO method is superior to the CP and TP methods, but that the TP method provides surprisingly good results. The CP method always leads to estimates of peak rates that are biased low. When F_{p*} is greater than 1.0, changes in both T_* and λ have little effect on D_* for the CP and TP inputs. This suggests that in high infiltration environments the hydraulic characteristics of both planes and channels play a secondary role in runoff generation. D_* decreases as T_*, F_{p*} and λ increase, but λ has little effect on D_* for the CP method. This is probably due to the fact that, with constant intensity input, the catchment outflow reaches an equilibrium rate for many of the storms in the set; thus, the peak rate distribution is little affected by catchment characteristics.

Spatially variable infiltration rate

Investigations of spatial infiltration variation were only carried out on a single flow plane, as incorporation of an impervious channel element would add little additional information. Results are presented first for a specific plane geometry and soil type for varying CV using the actual storm set (see cases 61–63 of Table 2; spatially variable infiltration rate). Results are then presented to illustrate the effect of CV on the distributions of runoff volume, time to peak, and peak rate produced by the three types of precipitation disaggregation. The outcome of a more detailed examination of the interaction of CV with specific storms of low, medium, and high intensity is then presented. Finally, the results

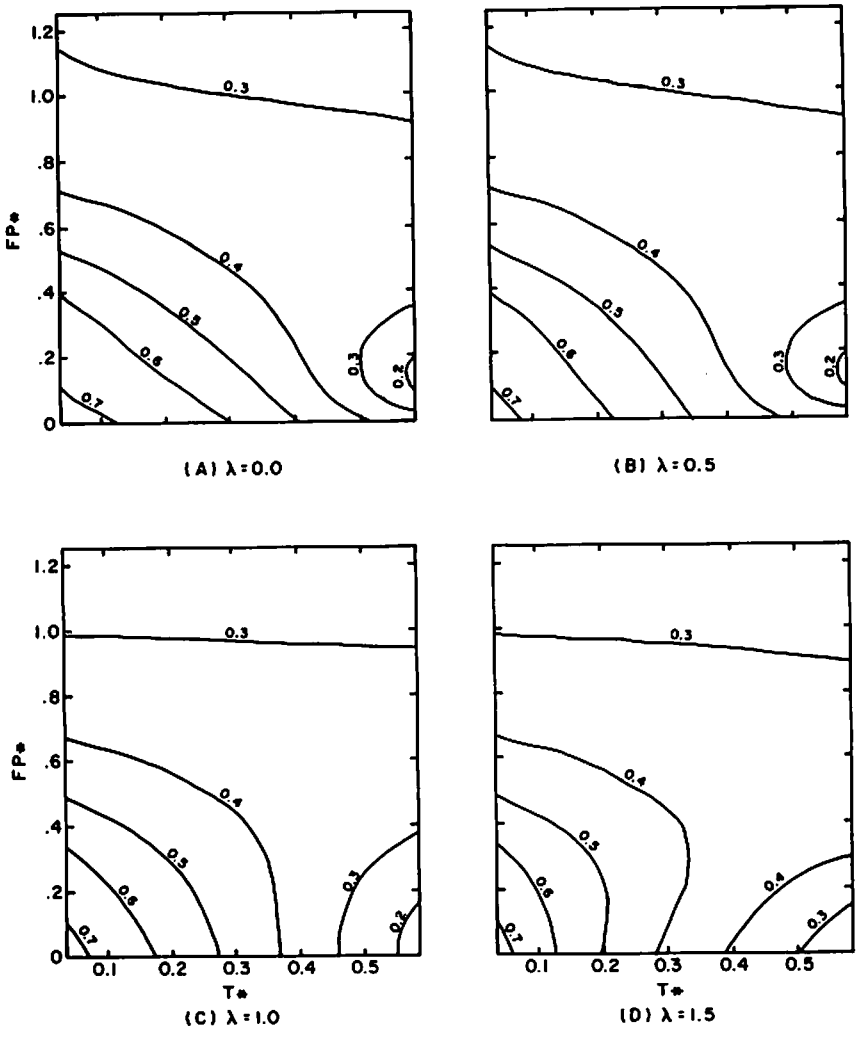

Fig. 7. Contour plots of the K-S D_n statistic for peak discharge from constant intensity input versus actual for: (a) $\lambda = 0.0$; (b) $\lambda = 0.5$; (c) $\lambda = 1.0$; (d) $\lambda = 1.5$.

indicating the errors one might incur when using the arithmetic mean instead of geometric mean for a uniformly infiltrating plane are offered.

The effects of spatial variability were studied at two levels by using a coefficient of variation of the $\ln(K_s')$ of 0.4 and 0.8. A survey of the literature indicated that these values are realistic and, in many cases, conservative (Rogowski, 1972; Nielsen et al., 1973; Sharma et al., 1980; Grah et al., 1983; Loague, 1986). These sources also support the assumption that the saturated hydraulic conductivity can be described by the lognormal distribution.

The actual storm set was applied to a 91.4 m plane with an effective saturated

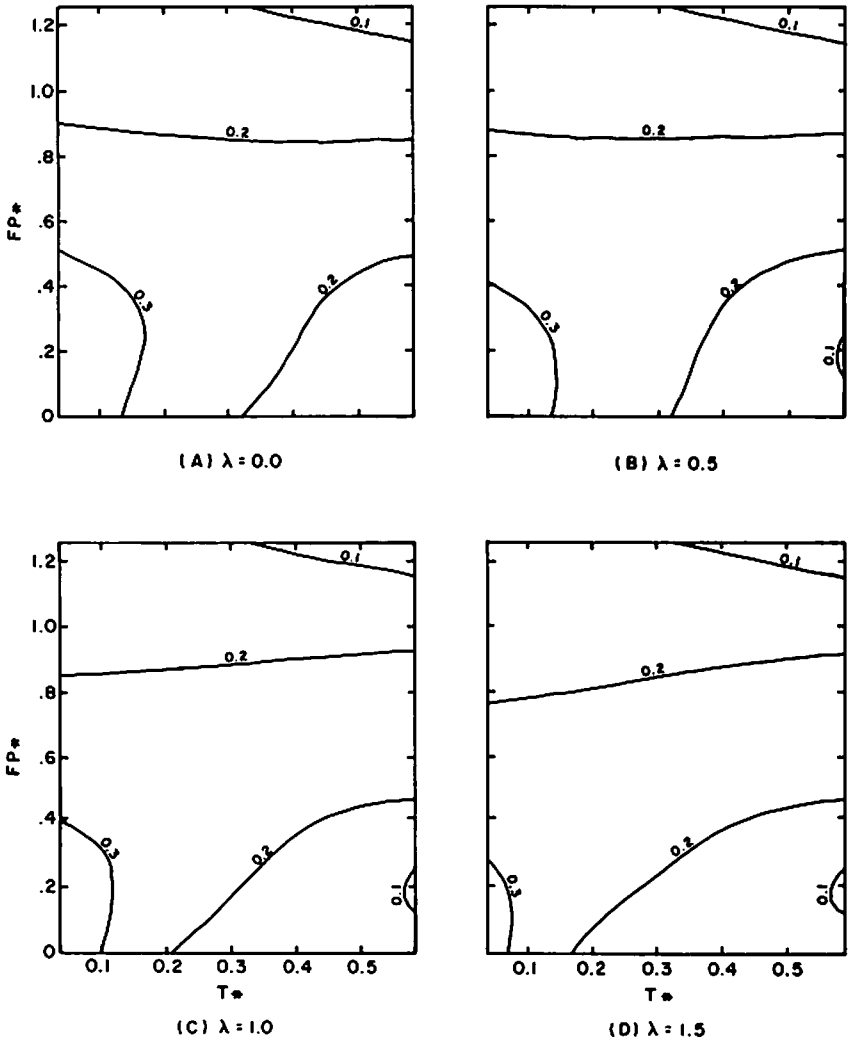

Fig. 8. Contour plots of the K–S D_n statistic for peak discharge from triangular intensity input versus actual for: (a) $\lambda = 0.0$; (b) $\lambda = 0.5$; (c) $\lambda = 1.0$; (d) $\lambda = 1.5$.

hydraulic conductivity $K_s' = 3.4\,\mathrm{mm\,h^{-1}}$ (geometric mean), and $CV = 0.0, 0.4$, and 0.8 to generate empirical distributions of runoff volume, time to peak, and peak rate. The CDFs are presented in Fig. 10. Increasing the spatial variation of infiltration (CV) increases the total runoff for the majority of the 30 rainfall events. The means of the time to peak decreased by increasing CV, and means of peak runoff rate increased with increasing CV.

Closer examination of Fig. 10 reveals a crossover of the CDFs for increasing CV. Summary statistics for the distributions bear out this observation by showing a decrease in the standard deviation of increasing CV. This trend

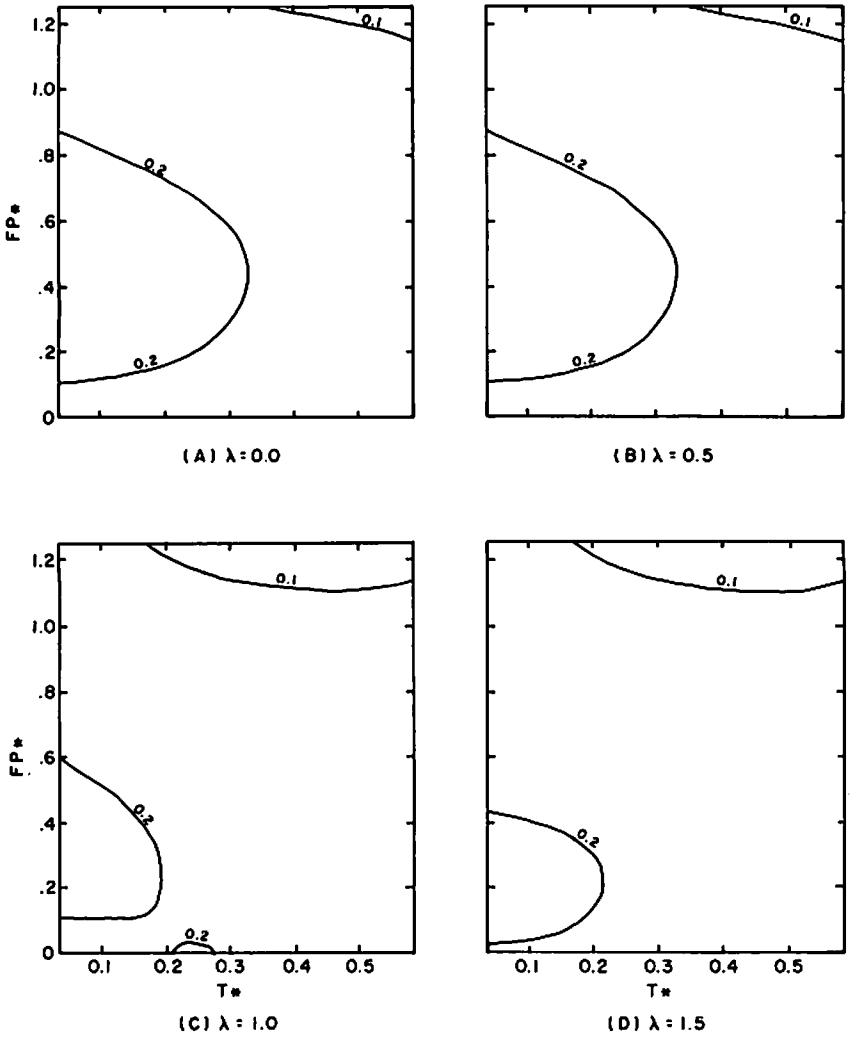

Fig. 9. Contour plots of the K-S D_* statistic for peak discharge from Woolhiser and Osborn disaggregation input versus actual for: (a) $\lambda = 0.0$; (b) $\lambda = 0.5$; (c) $\lambda = 1.0$; (d) $\lambda = 1.5$.

agrees with the findings of Freeze (1980), who stated that "a heterogeneous hillslope acts in a certain sense as an attenuating medium".

If the spatially variable infiltration does, in fact, dampen out precipitation variability, the K-S D_* statistic for comparing the distributions generated from disaggregated rainfall to the distributions generated from the actual storm should decrease as CV increases. Results from the cases examined in Table 2, spatially variable infiltration rate, indicate no consistent trend in the D_* statistics as a function of CV. The crossover of the empirical CDFs may be the cause of these inconsistencies, or the D_* statistic may not be a sensitive

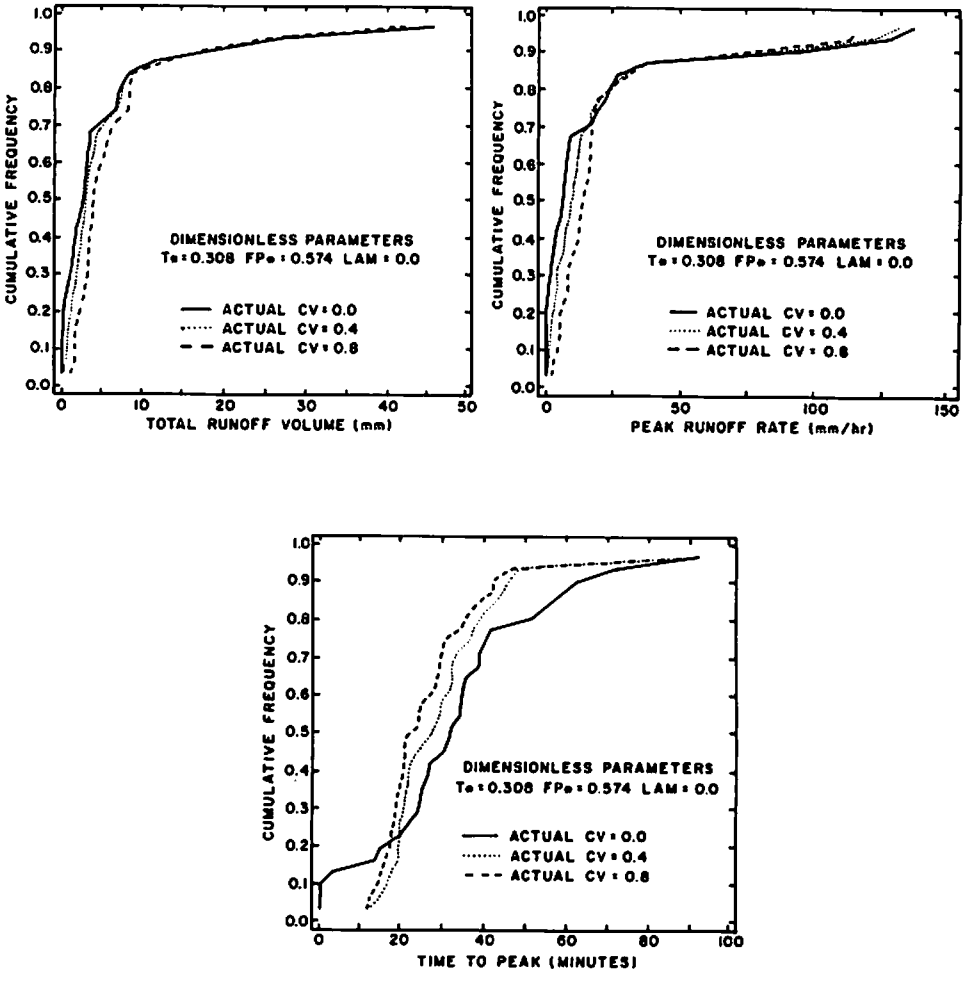

Fig. 10. Empirical CDFs of: (a) runoff volume; (b) peak rate; (c) time to peak from actual storms on a 91.4 m plane with spatially variable infiltration.

measure of distribution convergence. However, this analysis did show that, in cases of high infiltration (high F_{p*}), the number of runoff events increased as CV increased. This is expected, as the two portions of the runoff plane having a K_s' below the mean value (the lowest being nearly an order of magnitude smaller) will pond and produce runoff from relatively low intensity storms.

The inconclusive results relating D_* to CV prompted further investigation of the interaction between climate and spatial variability of infiltration. Three storms from the storm set of 30 were selected representing low, medium, and high weighted mean intensities. Table 3 presents statistics for the three selected storms.

These three actual storms were applied to a 91.4 m overland flow plane with

TABLE 3

Statistical characteristics of low-, medium-, and high-intensity selected storms

	Depth (mm)	Duration (min)	Peak intensity (mm h^{-1})	Weighted mean intensity (mm h^{-1})
Storm 1	23.9	44	64.8	33.6
Storm 4	19.6	95	34.5	18.8
Storm 30	75.9	61	289.6	74.9
Entire storm set (average)	25.9	47		

varying F_{p*} and CV (cases 58–66, Table 2), and the resulting hydrographs were plotted. Figure 11 shows the distinct interaction between the mean F_{p*} and C_v for storm 1. The crossover or reversal apparent in the CDF (Fig. 10) is shown in this figure as the spatially uniform plane (CV = 0.0) gives the highest peak rate for F_{p*} = 0.104, and the lowest peak rate when F_{p*} = 0.574. A composite schematic sketch of the response for cases 58–66, for each of the three storms, is presented in Fig. 12. This figure illustrates the climatic interaction with spatially varying infiltration.

At the lowest infiltration level (F_{p*} = 0.104), all three storms produce the largest peak when a uniformly infiltrating plane is used. For F_{p*} = 0.574, the largest storm also produces the largest peak on the uniform plane. This is not the case for the low and medium intensity storms, as the plane with the highest degree of spatially variable infiltration, CV = 0.8, produces the greatest peak.

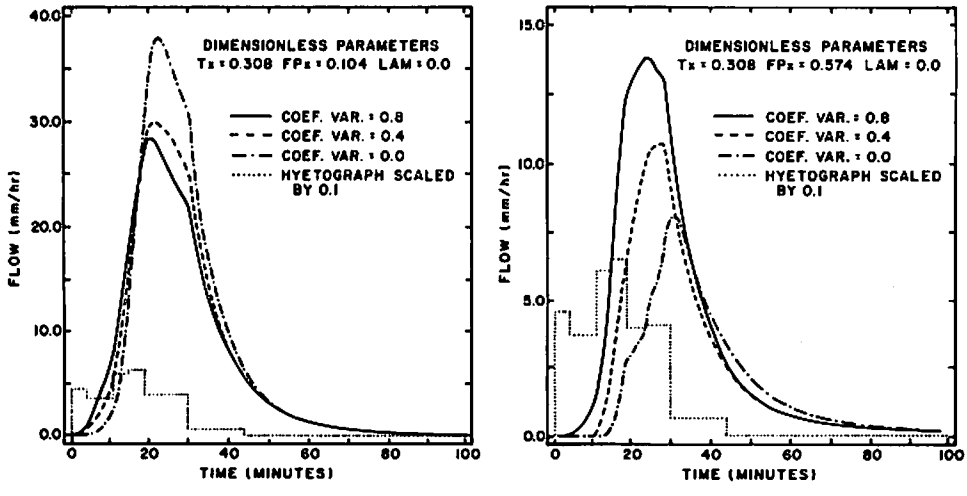

Fig. 11. Infiltration variability impact on the hydrographs from storm 1: (a) 91.4 m plane with small saturated hydraulic conductivity; (b) 91.4 m plane with medium saturated hydraulic conductivity.

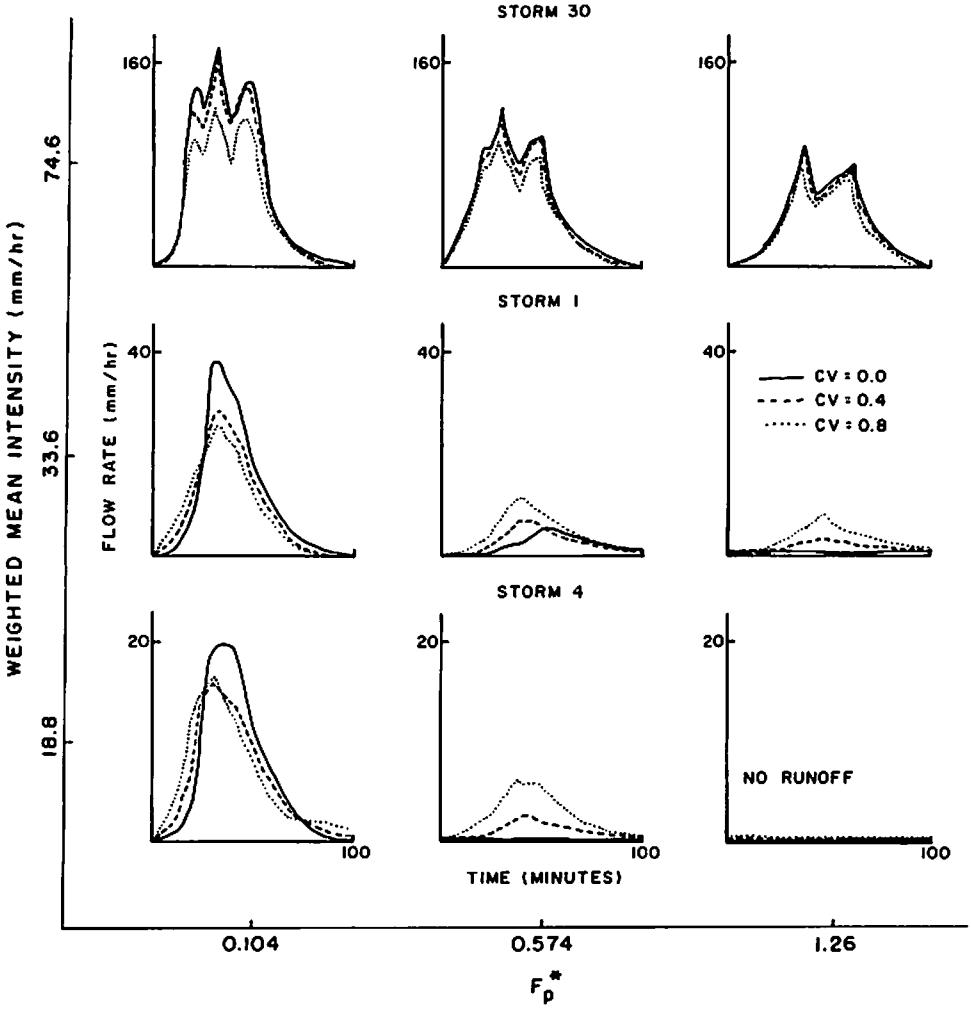

Fig. 12. Impacts of climate, degree of spatially variable infiltration (CV), and F_p on the hydrographs.

The same relative ordering of peak rates and runoff volumes also occurs at the highest infiltration level when $F_{p^*} = 1.26$.

To explain the reversals shown in Fig. 12, consider a constant intensity rainfall below the geometric mean of K_s', but above the lowest K_s' of the five plane segments for the spatially variable plane. In this case, the uniform plane will produce no runoff, but the spatially varying plane will. As the constant rainfall intensity level increases, the spatially variable plane will continue to produce more runoff than the uniform plane until the intensity reaches a certain level. Beyond this level (high intensity storms), the plane segments with high K_s' will dominate abstraction of rainfall from the spatially variable plane, and the uniform plane with geometric mean K_s' will produce more runoff.

Thus, the uniform plane will give higher peaks for low infiltration rates, or for large storms ($F_{p*} = 0.104$, or storm 30 in Fig. 12); while the spatially variable plane will produce larger peaks for higher geometric mean infiltration rates during low to medium intensity rainfall events.

DISCUSSION AND CONCLUSIONS

On average, the Woolhiser and Osborn (WO) precipitation disaggregation method is superior to isosceles and constant intensity disaggregation. However, when $F_{p*} \geqslant 0.4$, $T_* \geqslant 0.1$ and $\lambda \geqslant 1.5$, the isosceles disaggregation scheme will perform as well as the WO scheme. The constant intensity rainfall pattern cannot be recommended.

The results presented for the WO scheme were for a single realization of storms generated from a random seed. Study of ten additional realizations showed that random variation had a negligible effect on the computed K–S D_* statistic for empirical peak rate distribution functions although the upper tail of the CDF was affected substantially. The range of variation imparted by random variability was reduced substantially for only minor increases in basin damping response measures F_{p*}, T_*, and λ.

The channel effect on basin response, as measured by λ, was more significant for $\lambda \geqslant 0.5$. For $\lambda < 0.5$, the overland flow plane characteristics had a greater influence on watershed response. This agrees with the findings of Wooding (1965b). However, the range of λ studied does not substantially decrease the K–S D_* statistic between the CDFs generated from actual storms and those from disaggregated storms. Visual examination of Figs. 4 and 6 indicates that increasing λ does appear to increase distribution convergence, but D_* is apparently not sensitive to this level of convergence. D_* also does not appear to be sensitive to the damping caused by incorporating spatially variable infiltration.

These findings suggest that for the elementary channel system studied, the overland flow plane characteristics dominate watershed response due to Hortonian overland flow in a climate represented by the selected storm set. Visual examination of Golany and Larson's (1971) results reveal an unexpected increase in channel effect on basin response time when the transition is made from second- to third-order basins. Domination of basin response by channel characteristics will not likely occur for the elementary watershed system studied. Future work will address the order at which domination of basin response changes from overland flow to channel effects.

The results regarding spatial variability of K'_s shed new light on the findings of previous studies by Freeze (1980) and Smith and Hebbert (1979). Neither of these studies show the reversal of hydrographs for changing C_v of K'_s, as a function of climate and geometric mean K'_s, as shown in Fig. 12. The findings in this study more clearly point out the significance of the climatic-infiltration interaction, and warrant further investigation. Additional study also indicated

that significant differences in runoff behavior occur when the arithmetic mean is used instead of the geometric mean for the uniform K_s' case.

The overland runoff–runon problem was also investigated by Smith and Hebbert (1979). This case was not examined in this study, but they found if K_s increases upslope, less runoff and a greater damping of precipitation variability will result. Grah et al. (1983) produced experimental evidence on a Utah watershed showing that infiltration rate does increase upslope. It is not clear if this trend is solely the result of soil properties or depth to the saturated zone. If this trend commonly occurs, it would indicate that greater damping via spatially varying hydraulic conductivity would occur than is indicated by this study. Improvement in the K–S D_n statistics between the empirical CDFs resulting from the various precipitation intensity patterns examined may result if a runoff—runon study is undertaken. Future work should also investigate the effect of spatially varying vegetation, its interaction with infiltration rates, and its impact on runoff.

REFERENCES

Brakensiek, D.L., 1977. Estimating the effective capillary pressure in the Green and Ampt infiltration equation. Water Resour. Res., 13(3): 680–682.

Bras, R.L., 1979. Sampling of interrelated random fields: the rainfall–runoff case. Water Resour. Res., 15(6): 1767–1780.

Eagleson, P.S., 1972. Dynamics of flood frequency. Water Resour. Res., 8(4): 878–898.

Eagleson, P.S. and Shack, W.J., 1966. Some criteria for the measurement of rainfall and runoff. Water Resour. Res., 2(3): 427–436.

Engman, E.T. and Hershfield, D.M. 1981. Characterizing short duration rainfall intensities for runoff calculation. Trans. ASAE, (24SW): 347–352.

Freeze, R.A., 1980. A stochastic-conceptual analysis of rainfall–runoff processes on a hillslope. Water Resour. Res., 16(2): 391–408.

Golany, P. and Larson, C.L., 1971. Effects of channel characteristics on time parameters for small watershed runoff hydrographs. Water Resour. Res. Center, Univ. of Minn., Bull., 31: 104–118.

Grah, O.J., Hawkins, R.H. and Cundy, T.W., 1983. Distribution of infiltration on a small watershed. Adv. Irrig. Drain., pp. 44–54.

Harley, B.M., Perkins, F.E. and Eagleson, P.S., 1970. A modular distributed model of catchment dynamics. Ralph M. Parsons Lab., Dep. Civ. Eng., MIT, Cambridge, Mass., Rep. No. 133.

Hershenhorn, J.S., 1984. Disaggregation of daily rainfall. M.S. Thesis, Dep. Hydrol. ~~Water Resour.,~~ University of Arizona, Tucson, Ariz., 146 pp.

Hjelmfelf, A.T., Jr., 1981. Overland flow from time-distributed rainfall. J. Hydraul. Div., Am. Soc. Civ. Eng., 107 (HY2): 227–238.

Ishihara, T. and Takasao, T., 1963. A study on runoff pattern and its characteristics. Bull. Disaster Prev. Res. Inst., No. 65.

Iwagaki, Y. and Takasao, T., 1956. On the effects of rainfall and drainage-basin characteristics on runoff relation. Mem. Pap. 5th Anniv. Disaster Prev. Res. Inst., Kyoto Univ., pp. 191–200 (in Japanese).

Loague, K.M., 1986. An assessment of rainfall-runoff modeling methodology. Ph.D. Thesis, University of British Columbia, Vancouver, B.C., pp. 140–161.

Nielsen, D.R., Biggar, J.W. and Erh, K.T., 1973. Spatial variability of field measured soil-water properties. Hilgardia, 42(7): 215–260.

Rawls, W.J., Brakensiek, D.L. and Saxton, K.E., 1982. Estimation of soil water properties. Trans. Am. Soc. Agric. Eng., 25 SW: 1316–1320, 1328.

Rogowski, A.S., 1972. Watershed physics: soil variability criteria. Water Resour. Res., 8(4): 1015–1023.

Russo, D. and Bresler, E., 1981. Soil conductivity properties as stochastic processes: I. An analysis of field spatial variability. Soil Sci. Soc. Am., 45: 682–687.

Sharma, M.L., Gander, G.A. and Hunt, C.G., 1980. Spatial variability of infiltration in a watershed. J. Hydrol., 45: 101–122.

Smith, R.E. and Hebbert, R.H.B., 1979. A Monte Carlo analysis of the hydrologic effects of spatial variability of infiltration. Water Resour. Res., 15: 419–429.

Smith, R.E. and Parlange, J.Y., 1978. A parameter efficient hydrologic infiltration model. Water Resour. Res., 14(3): 533–538.

Srikanthan, R. and McMahon, T.A., 1985. Stochastic generation of rainfall and evaporation data. Aust. Water Resour. Counc., Tech. Pap. No. 894, Aust. Gov. Publ. Serv., Canberra, A.C.T., 301 pp.

Wooding, R.A., 1965a. A hydraulic model for the catchment-stream problem, I. Kinematic-wave Theory. J. Hydrol., 3: 254–267.

Wooding, R.A., 1965b. A hydraulic model for the catchment-stream problem, II. Numerical solutions. J. Hydrol., 3: 268–282.

Woolhiser, D.A., 1986. Sensitivity of calculated peak-runoff rates to rainfall-sampling frequency. In: Integrated Design of Hydrologic Networks. Proc., Budapest Symp., IAHS Publ., 158: 161–171.

Woolhiser, D.A. and Osborn, H.B., 1985. A stochastic model of dimensionless thunderstorm rainfall. Water Resour. Res., 21(4): 511–522.

Woolhiser, D.A., Osborn, H.B. and Hershenhorn, J.S., 1985. Disaggregation of daily rainfall. Proc. Nat. Resour. Modeling Symp., USDA-ARS Tech. Bull., ARS-30: 304–306.